Supporting Information

Xu et al. 10.1073/pnas.1406999111

SI Materials and Methods

Molecular Cloning. Benzenediol lactone synthese (BDLS) subunit pairs were produced in *Saccharomyces cerevisiae* BJ5464-NpgA (*MATα ura3-52 his3-Δ200 leu2-Δ1 trp1 pep4::HIS3 prb1 Δ1.6R can1 GAL*) (1, 2) using the compatible expression vectors YEpADH2p-FLAG-TRP and YEpADH2p-FLAG-URA for the intron-less highly reducing iterative polyketide synthase (hrPKS) and the nonreducing iterative polyketide synthase (nrPKS) genes, respectively (3). YEpCcRADS1, YEpCcRADS2, YEpAtCURS1, YEpAtCURS2, YEpLtLasS1, YEpLtLasS2, YEpAzResS1, and YEpAzResS2 were described previously (3–5).

The Udwary–Merski algorithm was used to predict domain boundaries in nrPKS (6). Considering that the AtCurS1–CcRadS2 heterologous iPKS pair provided no polyketide products even after the replacement of the starter unit:ACP transacylase (SAT) domain of CcRadS2 with $SAT_{AtCurS2}$ (YEpCcRadS2-$SAT_{AtCurS2}$), the domain replacement was repeated using a slightly shifted switchover site for the domain boundary (YEpCcRadS2-$SAT_{AtCurS2}$-B). Coexpressing this construct with YEpAtCurS1 also proved to be unproductive, indicating a fundamental incompatibility between the AtCurS1-generated priming unit and the CcRadS2 nrPKS.

The plasmid YEpCcRadS2-$SAT_{AtCurS2}$ is based on YEpADH2p-FLAG-URA and carries the intron-less *ccradS2* gene in which the gene segment encoding $SAT_{CcRadS2}$ was replaced by the one encoding $SAT_{AtCurS2}$. Using YEpAtCURS2 as the template, a 1,124-bp fragment encoding M^1–T^{362} of AtCurS2 was amplified with primers At_SAT_to_Cc_F (NdeI) and At_SAT_to_Cc_R. Using YEpCcRADS2 as a template, a 1,516-bp fragment encoding V^{367}-A^{871} of CcRadS2 was amplified with primers Cc_SAT_Dn_F and Cc_SAT_Dn_R (AgeI). These two PCR fragments were then fused using primers At_SAT_to_Cc_F (NdeI) and Cc_SAT_Dn_R (AgeI) and cloned into pJET1.2. After sequence verification, the NdeI–AgeI fragment was inserted into the equivalent cloning sites of YEpCcRADS2 to yield plasmid YEpCcRadS2-$SAT_{AtCURS2}$.

The plasmid YEpCcRadS2-$SAT_{AtCurS2}$-B is based on YEpADH2p-FLAG-URA and carries the intron-less *ccradS2* gene in which the gene segment encoding $SAT_{CcRadS2}$ was replaced by the one encoding $SAT_{AtCurS2}$. In comparison with the hybrid nrPKS produced by YEpCcRadS2-$SAT_{AtCurS2}$, this expression construct encodes a chimeric protein in which the switchover site is located four amino acids closer to the N terminus. Using YEpAtCURS2 as the template, a 1,111-bp fragment encoding M^1–T^{358} of AtCurS2 was amplified with primers SAT_Up_F (NdeI) and At_SAT_to_Cc_Up_R. Using YEpCcRADS2 as the template, a 1,553-bp fragment encoding Q^{364}–L^{880} of CcRadS2 was amplified with primers At_SAT_to_Cc_Dn_F and At_SAT_to_Cc_Dn_R (AgeI). These two PCR fragments were then fused using primers SAT_Up_F (NdeI) and At_SAT_to_Cc_Dn_R (AgeI) and cloned into pJET1.2. After sequence verification, the NdeI–AgeI fragment was inserted into the equivalent cloning sites of YEpCcRADS2 to yield plasmid YEpCcRadS2-$SAT_{AtCurS2}$-B.

The plasmid YEpYX24 is based on YEpADH2p-FLAG-URA and carries the intron-less *atcurS2* gene in which the gene segment encoding $SAT_{AtCurS2}$ was replaced by the one encoding $SAT_{CcRadS2}$ (7). Using YEpCcRADS2 as the template, a 1,125-bp fragment encoding M^1–S^{366} of CcRadS2 was amplified with primers Cc_SAT_to_At_F (NdeI) and Cc_SAT_to_At_R. Using YEpAtCURS2 as the template, a 1,059-bp fragment encoding P^{363}–N^{714} of AtCurS2 was amplified with primers At_SAT_Dn_F and At_SAT_Dn_R (Bsu36I). These two PCR fragments were then fused using primers Cc_SAT_to_At_F (NdeI) and At_SAT_Dn_R (Bsu36I) and cloned into pJET1.2. After sequence verification, the NdeI–Bsu36I fragment was inserted into the equivalent cloning sites of YEpAtCURS2 to yield plasmid YEpYX24.

The plasmid YEpLtLasS2-$SAT_{CcRadS2}$ is based on YEpADH2p-FLAG-URA and carries the intron-less *ltlasS2* gene in which the gene segment encoding $SAT_{LtLasS2}$ was replaced by the one encoding $SAT_{CcRadS2}$. Using YEpCcRADS2 as the template, a 1,147-bp fragment encoding M^1–S^{366} of CcRadS2 was amplified with primers SAT_Up_F (NdeI) and Cc_SAT_Up_R. Using YEpLtLasS2 as the template, a 1,298-bp fragment encoding L^{355}—C^{786} of LtLasS2 was amplified with primers Lass_Dn_F and Lass_Dn_R (HpaI). These two PCR fragments were then fused using primers SAT_Up_F (NdeI) and Lass_Dn_R (HpaI) and cloned into pJET1.2. After sequence verification, the NdeI–HpaI fragment was inserted into the equivalent cloning sites of YEpLtLasS2 to yield plasmid YEpLtLasS2-$SAT_{CcRadS2}$.

The plasmid YEpLtLasS2-$SAT_{AtCurS2}$ is based on YEpADH2p-FLAG-URA and carries the intron-less *ltlasS2* gene in which the gene segment encoding $SAT_{LtLasS2}$ was replaced by the one encoding $SAT_{AtCurS2}$. Using YEpAtCURS2 as the template, a 1,123-bp fragment encoding M^1–A^{358} of AtCurS2 was amplified with primers SAT_Up_F (NdeI) and At_SAT_Up_R. Using YEpLtLasS2 as the template, a 1,298-bp fragment encoding L^{355}–C^{786} of LtLasS2 was amplified with primers Lass_Dn_F and Lass_Dn_R (HpaI). These two PCR fragments were then fused using primers SAT_Up_F (NdeI) and Lass_Dn_R (HpaI) and cloned into pJET1.2. After sequence verification, the NdeI–HpaI fragment was inserted into the equivalent cloning sites of YEpLtLasS2 to yield plasmid YEpLtLasS2-$SAT_{AtCurS2}$.

The plasmid YEpLtLasS2-$SAT_{AzResS2}$ is based on YEpADH2p-FLAG-URA and carries the intron-less *ltlasS2* gene in which the gene segment encoding $SAT_{LtLasS2}$ was replaced by the one encoding $SAT_{AzResS2}$. Using YEpAzResS2 as the template, a 1,222-bp fragment encoding M^1–D^{391} of AzResS2 was amplified with primers SAT_Up_F (NdeI) and Ress_SAT_Up_R. Using YEpLtLasS2 as the template, a 1,298-bp fragment encoding L^{355}–C^{786} of LtLasS2 was amplified with primers Lass_Dn_F and Lass_Dn_R (HpaI). These two PCR fragments were then fused using primers SAT_Up_F (NdeI) and Lass_Dn_R (HpaI) and cloned into pJET1.2. After sequence verification, the NdeI–HpaI fragment was inserted into the equivalent cloning sites of YEpLtLasS2 to yield plasmid YEpLtLasS2-$SAT_{AzResS2}$.

Heterologous Production and Isolation of Polyketides. A freshly prepared liquid culture of the appropriate yeast strain in synthetic complete (SC) medium [0.67% yeast nitrogen base, 2% (wt/vol) glucose, and 0.72 g/L appropriate dropout supplement] was used as the inoculum for typical large-scale fermentations. Twenty 250-mL Erlenmeyer flasks, each containing 50 mL of SC medium, were inoculated with 0.5 mL of seed culture and cultivated for 16–24 h at 30 °C with shaking at 300 rpm (New Brunswick Innova G25 incubator shaker). After the OD_{600} of the culture reached 1.0, 50 mL of yeast extract–peptone medium [1% yeast extract and 2% (wt/vol) peptone] was added to each flask, and the cultivation was continued for 72 h. The cultures were combined, adjusted to pH 5.0, and extracted with 2 L of EtOAc three times. The EtOAc extract was evaporated to dryness under vacuum, loaded to a Diaion HP-20 column (4 × 30 cm), and successively eluted with H_2O, 25% (vol/vol) MeOH/H_2O, and

acetone. The acetone fraction was collected and further separated by HPLC using an Eclipse XDB C18 column (5 μm, 4.6 × 150 mm) or/and an Eclipse Plus C8 column (5 μm, 4.6 × 150 mm).

Compound **1** (monocillin II, 1.8 mg) was purified from the acetone fraction of the extract of *S. cerevisiae* BJ5464-NpgA [YEpCcRadS1, YEpAzResS2] by HPLC using an Eclipse XDB C18 column [52% (vol/vol) CH_3CN/H_2O, 1 mL/min]. Compound **6** was isolated on an Eclipse XDB C18 column [58% (vol/vol) CH_3CN/H_2O, 1 mL/min] from both of the strains *S. cerevisiae* BJ5464-NpgA [YEpLtLasS1, YEpAzResS2] (15.0 mg) and *S. cerevisiae* BJ5464-NpgA [YEpLtLasS1, YEpCcRadS2] (4.1 mg). Compounds **3** (8.4 mg), **10** (3.6 mg), and **11** (3.2 mg) were purified from strain *S. cerevisiae* BJ5464-NpgA [YEpAzResS1, YEpCcRadS2] by separation of the acetone fraction on an Eclipse XDB C18 column [41% (vol/vol) CH_3CN/H_2O, 1 mL/min] and an Eclipse Plus C8 column [33% (vol/vol) CH_3CN/H_2O, 1 mL/min]. Compound **12** (3.7 mg) was isolated from *S. cerevisiae* BJ5464-NpgA [YEpCcRadS1, YEpLtLasS2-$SAT_{CcRadS2}$] by HPLC separation of the acetone fraction on an Eclipse XDB C18 column [49% (vol/vol) CH_3CN/H_2O, 1 mL/min]. Compounds **13** (10.5 mg) and **14** (8.5 mg) were acquired from strain *S. cerevisiae* BJ5464-NpgA [YEpAzResS1, YEpLtLasS2-$SAT_{AzResS2}$] through an Eclipse XDB C18 column [40% (vol/vol) CH_3CN/H_2O, 1 mL/min]. Compounds **15** (2.8 mg) and **16** (3.2 mg) were both from strain *S. cerevisiae* BJ5464-NpgA [YEpAzResS1, YEpAtCurS2] by the separation of acetone fraction on an Eclipse XDB C18 column [42% (vol/vol) CH_3CN/H_2O, 1 mL/min]. Compound **17** (6.6 mg) was obtained from strain *S. cerevisiae* BJ5464-NpgA [YEpLtLasS1, YEpAtCurS2] through an Eclipse XDB C18 column [47% (vol/vol) CH_3CN/H_2O, 1 mL/min]. Compound **18** (radilarin) was produced by strain *S. cerevisiae* BJ5464-NpgA [YEpCcRadS1, YEpYX24] with a yield of 9 mg/L, as previously reported (7).

Chemical Characterization of Polyketide Products. Optical rotations were recorded on a Rudolph Autopol IV polarimeter with a 10-cm cell. Circular dichroism (CD) spectra were acquired with a JASCO J-810 instrument using a path length of 1 cm. ^1H, ^{13}C, and 2D NMR spectra, including proton–proton correlation spectroscopy (^1H-^1H COSY), heteronuclear single quantum coherence, heteronuclear multiple bond correlation (HMBC), and rotating-frame nuclear Overhauser effect spectroscopy (ROESY) spectra were recorded in DMSO-d_6, CD_3OD, or C_5D_5N on a JEOL ECX-300 spectrometer (δ in ppm, *J* in Hz). Electrospray ionization (ESI) MS data were collected on an Agilent 6130 single quadrupole liquid chromatography (LC) MS equipment.

All of the compounds were subjected to spectroscopic analyses for structure elucidation. Comparison of the spectroscopic data with those reported allowed compounds **1, 2, 3, 4, 5, 6, 7, 15**, and **18** (Fig. S2) to be identified as monocillin II, *trans*-resorcylide, YXTZ-53-51-251, desmethyl-lasiodiplodin, *R*-zearalane, lasicicol, 10,11-dehydro-15(*S*)-curvularin, 10,11-dehydro-15(*R*)-curvularin, and radilarin, respectively (5, 7–10). Compounds **8** and **9** were characterized by LC-MS analysis and coinjection with authentic samples as the known isocoumarins YXTZ-3-16-2 and YXTZ-3-15 isolated during our previous work (4, 7).

Compound **10** showed similar UV (Fig. S3), ^1H NMR, and ^{13}C NMR data (Table S2) to those of YXTZ-3-49-4 (7). The ESI-MS spectrum of **10** showed the $[M-H]^-$ ion peak at *m/z* 335.2 and $[M+H]^+$ at *m/z* 336.9, suggesting that the molecular weight of this compound is 336. 2D NMR (Fig. S4) confirmed that it has a planar structure identical to YXTZ-3-49-4. The stereostructure of this compound was deduced from ROESY correlations and the biosynthetic pathway. The biosynthetic origin of **10** supported that the absolute configuration at C-15 is *R*, which is the same as **3** isolated from this strain. The ROESY correlation of H-11 to H-15 (Fig. S4) indicated that both protons are on the same side. Accordingly, the configuration at C-11 was deduced to be *R*. Therefore, the structure of **10** was elucidated as ethyl 2,4-dihydroxy-6-(3-((2*R*,6*R*)-6-methyltetrahydro-2*H*-pyran-2-yl)-2-oxopropyl)benzoate, and the compound was named YXTZ-2-53-c.

ESI-MS showed that compound **11** has a molecular weight of 336, which is two mass units greater than that of **3**, suggesting that it is a reduced analog of **3**. Its NMR spectra is similar to those of **3** except H-10 at δ_H 2.67 (1H, dd, 14.8, 4.5) and δ_H 2.54 (1H, dd, 14.8, 8.2), and the H-11 signal at δ_H 3.96 (1H, m) and δ_C 68.5. At the same time, the signal for the C-11 ketone group in the ^{13}C NMR spectrum of **3** was not found in that of **11**. These observations indicate that **11** is generated from **3** by reduction of the C-11 ketone group to a hydroxyl group. The structure of **11** was confirmed by 2D NMR (Fig. S4) to be 3-(2,8-dihydroxynonyl)-6,8-dihydroxy-1H-isochromen-1-one. The configuration at C-15 was deduced to be *R* from its biosynthetic origin, which is same as **3** and **10**. This compound was named as YXTZ-2-53-e.

Compound **12** was isolated as a white solid with a resorcylide-type UV spectrum (Fig. S3). ESI-MS revealed that its molecular weight is 274, four mass units less than desmethyl-lasiodiplodin. The proton signals at δ_H 6.64 (1H, d, 15.6), 6.59 (1H, dt, 15.6, 5.8) and 5.40 (2H, m) indicated that two olefinic bonds are present. The ^1H-^1H COSY and HMBC correlations (Fig. S4) allowed these two olefinic bonds to be assigned to C-8/C-9 and C-12/C-13. Positive Cotton effect at $\delta\varepsilon_{270}$ +4.25 indicated the *R* configuration of C-15. The structure of **12** was thus determined to be (*R*,5*E*,9*E*)-12,14-dihydroxy-3-methyl-3,4,7,8-tetrahydro-1*H*-benzo[*c*][1]oxacyclododecin-1-one, and the compound was named radiplodin.

Compound **13** shows an UV absorption spectrum similar to those of acyl resorcylic acid esters (Fig. S3). The molecular weight of this compound was determined to be 294 based on the ion peaks $[M-H]^-$ at *m/z* 292.8 and $[M+H]^+$ at *m/z* 295.2. The ^1H NMR spectrum showed signals for one olefinic bond at δ_H 6.11 (1H, d, 15.4) and 6.60 (1H, m). It also revealed signals for one oxygenated CH group at δ_H 4.02 (1H, m), which belong to H-8, H-9 and H-13 in the C-7 side chain based on the ^1H-^1H COSY and HMBC spectra (Fig. S4). The attachment of the side chain to C-7 and the presence of the ester bond were confirmed by the HMBC correlations shown in Fig. S4. Inspection of the Δδ value (+0.04) of 14-CH_3 (Fig. S5) from Mosher's reactions allowed the absolute configuration at C-13 to be established as *R*. **13** was thus unambiguously identified as (*R*,*E*)-ethyl 2,4-dihydroxy-6-(6-hydroxyhept-1-en-1-yl)benzoate, and the compound was named YXTZ-53-77-b.

Compound **14** has the characteristic UV absorption spectrum of an isocoumarin (Fig. S3) and a molecular weight of 290. The ^1H NMR spectrum is similar to that of YXTZ-3-16-2 reported previously (2). The ^{13}C NMR spectrum (Table S3) showed 16 carbon signals, just as for YXTZ-3-16-2. The 2D NMR spectra (Fig. S4) further confirmed that **14** and YXTZ-3-16-2 have the same planar structure. The absolute configuration at C-15 was determined to be *R* based on the Δδ value (+0.07) of 16-CH_3 from Mosher's reactions (Fig. S5). Compound **14** was thus identified as (*R*,*E*)-6,8-dihydroxy-3-(6-hydroxyhept-1-en-1-yl)-1*H*-isochromen-1-one. This compound was previously isolated from *S. cerevisiae* BJ5464-NpgA [YEpAzResS1, YEpAzResS2] as YXTZ-53-51-322, and its configuration at C-15 was proposed to be *R* based on the biosynthetic origin (1). The current work unambiguously determined the absolute configuration of this compound at C-15.

Compound **16** was proposed to be a curvularin-type macrolactone based on its UV spectrum (Fig. S3). The ion peaks in the ESI-MS spectra included $[M-H]^-$ at *m/z* 317.0 and $[M+H]^+$ at *m/z* 319.0, indicating that the molecular weight of this compound is 318. The ^{13}C NMR spectrum revealed the presence of 18 carbon atoms (Table S3). A double bond was assigned to C-10 and C-11 on the basis of HMBC and ^1H-^1H COSY correlations (Fig. S4). Positive Cotton effect at $\delta\varepsilon_{226}$ +1.09 indicated the *R* configuration at C-17. The structure of **16** was therefore

characterized as (*R*,*E*)-13,15-dihydroxy-4-methyl-4,5,6,7,8,9-hexahydro-1*H*-benzo[*d*][1]oxacyclotetradecine-2,12-dione, and the compound was named 14,15-dihydroradilarin.

Compound **17** also showed a UV spectrum (Fig. S3) similar to that of curvularin. The molecular weight was determined to be 320 based on the ion peaks $[M-H]^-$ at *m/z* 319.0 and $[M+H]^+$ at *m/z* 321.0 in the ESI-MS spectra, two mass units greater than **16**. Similar to **16**, the ^{13}C NMR spectrum revealed the presence of 18 carbon atoms in **17** (Table S3). No olefinic signals were observed in the ^1H and ^{13}C NMR spectra, consistent with the two mass units difference between **16** and **17**, which is a result of the reduction of the C-10/C-11 double bond. The HMBC correlations of H-2 at δ_H 3.95 (1H, d, 17.1) and 3.52 (1H, d, 17.1) to C-1, C-3 and C-4 confirmed that **17** has a dihydroxyphenylacetic acid lactone structure like curvularin and **16**. Further, ^1H-^1H COSY and HMBC analysis (Fig. S4) allowed this structure to be characterized as the 18-carbon macrolactone shown in Fig. S2. The absolute configuration at C-15 was deduced to be *R* according to the Cotton effect at $\delta\varepsilon_{264}$ +3.63 in the CD spectrum. Thus, the structure of **17** was elucidated as (*R*)-13,15-dihydroxy-4-methyl-4,5,6,7,8,9,10,11-octahydro-1*H*-benzo[d][1]oxacyclotetradecine-2,12-dione, and the compound was named lasilarin.

Compound **10**: white amorphous solid; UV: see Fig. S3; $[\alpha]_D$ = -52.7° (*c* 0.06, MeOH); ^1H NMR and ^{13}C NMR (CD_3OD): see Table S2 and Figs. S7 and S8; ESI-MS (*m/z*): 335.2 $[M-H]^-$, 336.9 $[M+H]^+$.

Compound **11**: white amorphous solid; UV: see Fig. S3; $[\alpha]_D$ = +10.9° (*c* 0.17, MeOH); ^1H NMR and ^{13}C NMR (CD_3OD): see Table S2 and Figs. S9 and S10; ESI-MS (*m/z*): 335.2 $[M-H]^-$, 336.9 $[M+H]^+$, 359.0 $[M+Na]^+$.

Compound **12**: white amorphous solid; UV: see Fig. S3; $[\alpha]_D$ = +22.7° (*c* 0.18, MeOH); ^1H NMR and ^{13}C NMR (CD_3OD): see Table S2 and Figs. S11 and S12; CD $\delta\varepsilon_{221}$ -4.77, $\delta\varepsilon_{270}$ +4.25 (1.8 mM in MeOH); ESI-MS (*m/z*): 272.7 $[M-H]^-$, 275.0 $[M+H]^+$.

Compound **13**: white amorphous solid; UV: see Fig. S3; $[\alpha]_D$ = +20.7° (*c* 0.30, MeOH); ^1H NMR and ^{13}C NMR (CD_3OD): see Table S3 and Figs. S13 and S14; ESI-MS (*m/z*): 292.8 $[M-H]^-$, 295.2 $[M+H]^+$.

Compound **14**: white amorphous solid; UV: see Fig. S3; $[\alpha]_D$ = -12.4° (*c* 0.11, MeOH); ^1H NMR and ^{13}C NMR (pyridine-d_5): see Table S3 and Figs. S15 and S16; ESI-MS (*m/z*): 289.0 $[M-H]^-$, 291.1 $[M+H]^+$, 313.2 $[M+Na]^+$.

Compound **15**: white amorphous solid; $[\alpha]_D$ = +60.0° (*c* 0.11, MeOH); UV: see Fig. S3; ^1H NMR (300 MHz, CD_3OD): δ 6.65 (1H, d, *J* = 15.4 Hz, H-10), 6.52 (1H, m, H-11), 6.18 (1H, d, *J* = 2.0 Hz, H-4), 6.11 (1H, d, *J* = 2.0 Hz, H-6), 4.80 (1H, m, H-15), 3.88 (1H, d, *J* = 17.2 Hz, H-2a), 3.46 (1H, d, *J* = 17.2 Hz, H-2b), 2.37 (2H, m, H_2-12), 1.61 (2H, m, H_2-13), 1.94 (2H, m, H_2-14), 1.21 (3H, d, *J* = 6.1 Hz, H_3-16); ^{13}C NMR (75 MHz, CD_3OD): δ 172.6 (C-1), 43.2 (C-2), 136.8 (C-3), 112.2 (C-4), 163.0 (C-5), 103.0 (C-6), 163.5 (C-7), 118.2 (C-8), 198.3 (C-9), 132.6 (C-10), 153.1 (C-11), 34.7 (C-12), 33.0 (C-13), 25.4 (C-14), 73.7 (C-15), 20.6 (C-16); CD $\delta\varepsilon_{193}$ -1.65, $\delta\varepsilon_{228}$ +2.68, $\delta\varepsilon_{273}$ −1.41, $\delta\varepsilon_{293}$ −0.38, $\delta\varepsilon_{299}$ −0.47, $\delta\varepsilon_{326}$ +1.27 (0.9 mM in MeOH); ESI-MS (*m/z*): 289.0 $[M-H]^-$, 291.0 $[M+H]^+$.

Compound **16**: white amorphous solid; UV: see Fig. S3; $[\alpha]_D$ = -8.6° (*c* 0.04, MeOH); ^1H NMR and ^{13}C NMR (CD_3OD): see Table S3 and Figs. S17 and S18; CD $\delta\varepsilon_{196}$ -2.79, $\delta\varepsilon_{218}$ +1.00, $\delta\varepsilon_{226}$ +1.09, $\delta\varepsilon_{245}$ -1.48, $\delta\varepsilon_{272}$ -0.39, $\delta\varepsilon_{308}$ +0.54 (1.6 mM in MeOH); ESI-MS (*m/z*): 317.0 $[M-H]^-$, 319.0 $[M+H]^+$.

Compound **17**: white amorphous solid; UV: see Figure S3; $[\alpha]_D$ = -51.4° (*c* 0.28, MeOH); ^1H NMR and ^{13}C NMR (CD_3OD): see Table S3 and Figs. S19 and S20; CD $\delta\varepsilon_{215}$ +3.88, $\delta\varepsilon_{235}$ -1.15, $\delta\varepsilon_{264}$ +3.63, $\delta\varepsilon_{285}$ +0.64, $\delta\varepsilon_{294}$ +0.70, $\delta\varepsilon_{321}$ -4.64 (1.6 mM in MeOH); ESI-MS (*m/z*): 319.0 $[M-H]^-$, 321.0 $[M+H]^+$.

Preparation of Mosher Ester Derivatives of 13 and 14. A measurement of 0.5 mg of **13** or **14** was transferred into a clean and completely dry NMR tube. Deuterated pyridine (0.5 mL) and (*S*)-(+)-α-methoxy-α-(trifluoromethyl)phenylacetyl chloride [(*S*)-MTPA-Cl)] (6 μL) were added to each NMR tube immediately, and the tubes were shaken carefully to evenly mix the sample with (*S*)-MTPA-Cl. The reaction mixtures were incubated at 15 °C for 12 h to yield the MTPA esters **13R** and **14R**, respectively. The esters **13S** and **14S** were obtained similarly by reacting the respective compound with (*R*)-MTPA-Cl. Δδ values ($\delta_S - \delta_R$) were calculated and are shown in Fig. S5.

1. Ma SM, et al. (2009) Complete reconstitution of a highly reducing iterative polyketide synthase. *Science* 326(5952):589–592.
2. Lee KK, Da Silva NA, Kealey JT (2009) Determination of the extent of phosphopantetheinylation of polyketide synthases expressed in *Escherichia coli* and *Saccharomyces cerevisiae*. *Anal Biochem* 394(1):75–80.
3. Xu Y, et al. (2013) Characterization of the biosynthetic genes for 10,11-dehydrocurvularin, a heat shock response-modulating anticancer fungal polyketide from Aspergillus terreus. *Appl Environ Microbiol* 79(6):2038–2047.
4. Xu Y, et al. (2013) Rational reprogramming of fungal polyketide first-ring cyclization. *Proc Natl Acad Sci USA* 110(14):5398–5403.
5. Xu Y, et al. (2014) Insights into the biosynthesis of 12-membered resorcylic acid lactones from heterologous production in *Saccharomyces cerevisiae*. *ACS Chem Biol* 9(5):1119–1127.
6. Udwary DW, Merski M, Townsend CA (2002) A method for prediction of the locations of linker regions within large multifunctional proteins, and application to a type I polyketide synthase. *J Mol Biol* 323(3):585–598.
7. Xu Y, et al. (2013) Thioesterase domains of fungal nonreducing polyketide synthases act as decision gates during combinatorial biosynthesis. *J Am Chem Soc* 135(29):10783–10791.
8. Greve H, et al. (2008) Apralactone A and a new stereochemical class of curvularins from the marine fungus. *Curvularia* sp. *Eur J Org Chem* 2008:5085–5092.
9. Dai J, et al. (2010) Curvularin-type metabolites from the fungus Curvularia sp. isolated from a marine alga. *Eur J Org Chem* 2010(36):6928–6937.
10. Arai K, Rawlings BJ, Yoshizawa Y, Vederas JC (1989) Biosyntheses of antibiotic A26771B by *Penicillium turbatum* and dehydrocurvularin by *Alternaria cinerariae*: comparison of stereochemistry of polyketide and fatty acid enoyl thiol ester reductases. *J Am Chem Soc* 111(9):3391–3399.

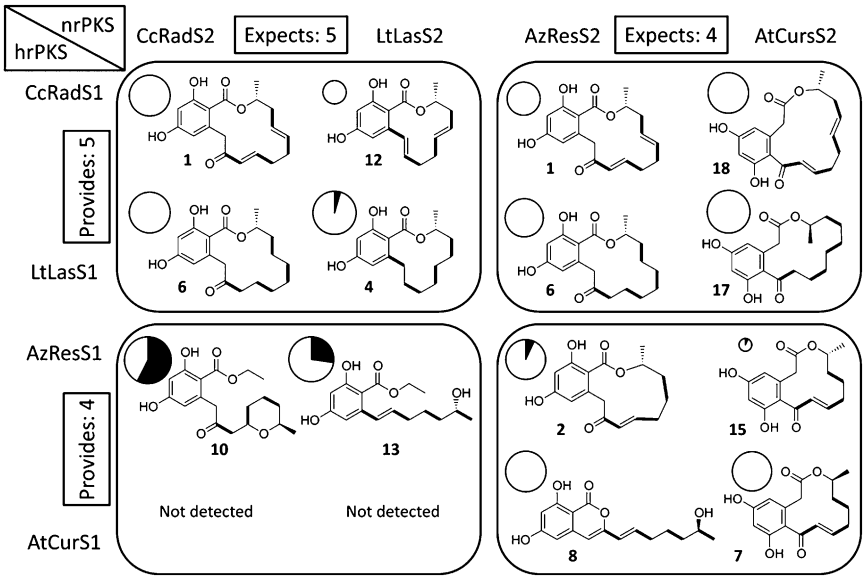

Fig. S1. Combinatorial biosynthesis of benzenediol lactones and their congeners. Combinatorial matrix view of the main on-program products of BDLS subunit heterocombinations. The length of the biosynthon provided by the hrPKSs and the length of the native biosynthon expected by the nrPKSs are shown as the number of malonyl-CoA units incorporated (five for a pentaketide, four for a tetraketide). Pie charts illustrate the relative production of on-program (white) and stutter products (black), with the size of the pie proportional to the total polyketide titers.

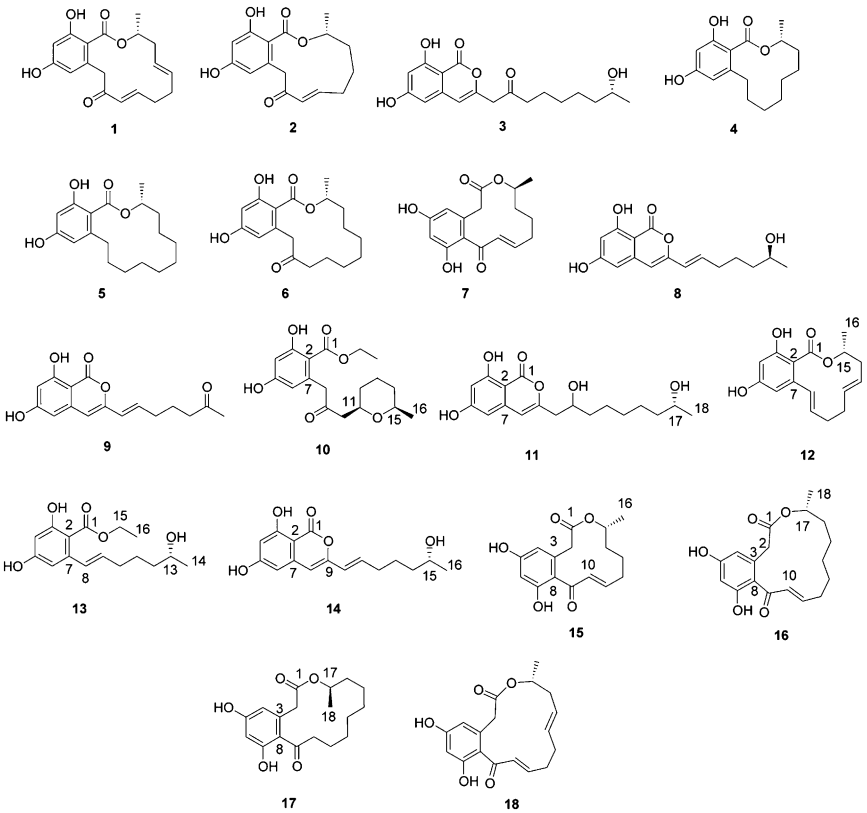

Fig. S2. Chemical structures of **1–18**.

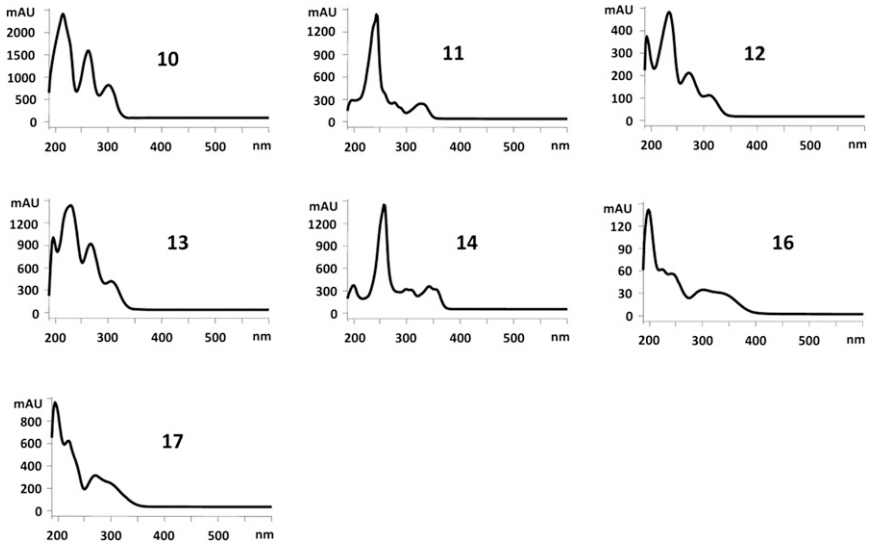

Fig. S3. UV spectra of **10, 11, 12, 13, 14, 16**, and **17**.

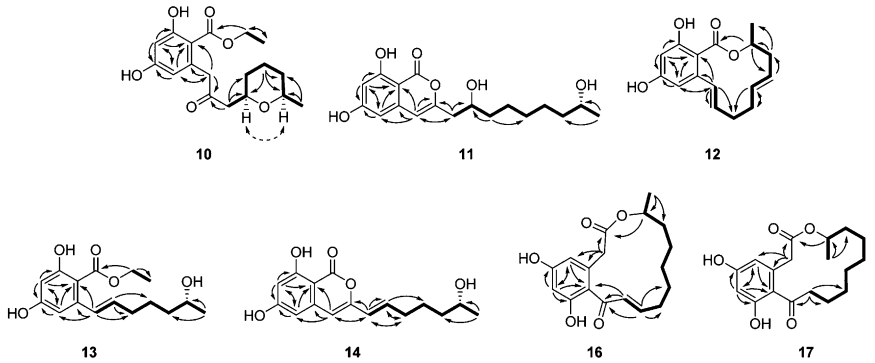

Fig. S4. Key HMBC (⟶), ^{1}H-^{1}H-COSY (▬), and ROESY (⇠⇢) correlations for **10, 11, 12, 13, 14, 16**, and **17**.

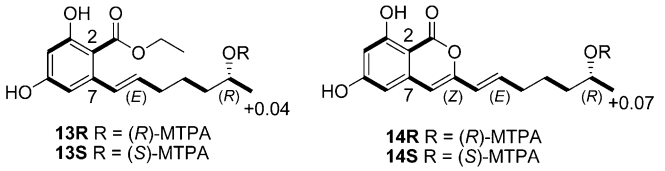

Fig. S5. Δδ values [(Δδ in ppm) = $\delta_S - \delta_R$] obtained for (*S*)- and (*R*)-MTPA esters of **13** and **14**.

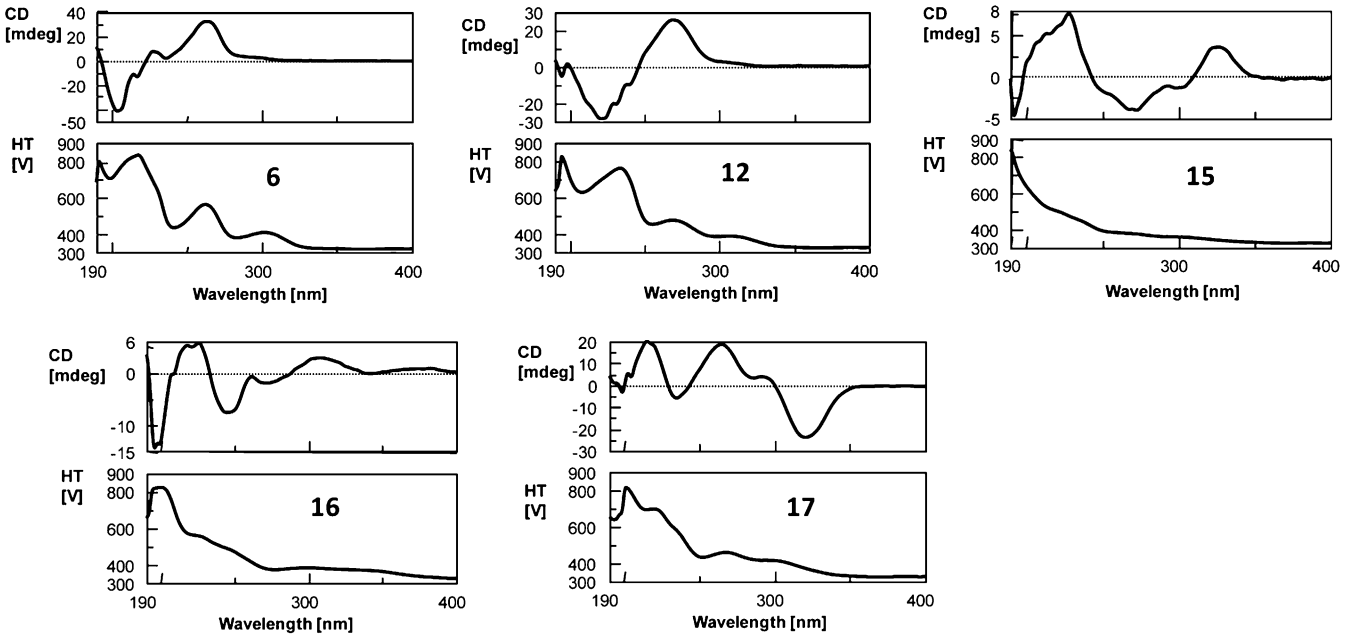

Fig. S6. CD and UV spectra of **6, 12, 15, 16**, and **17**.

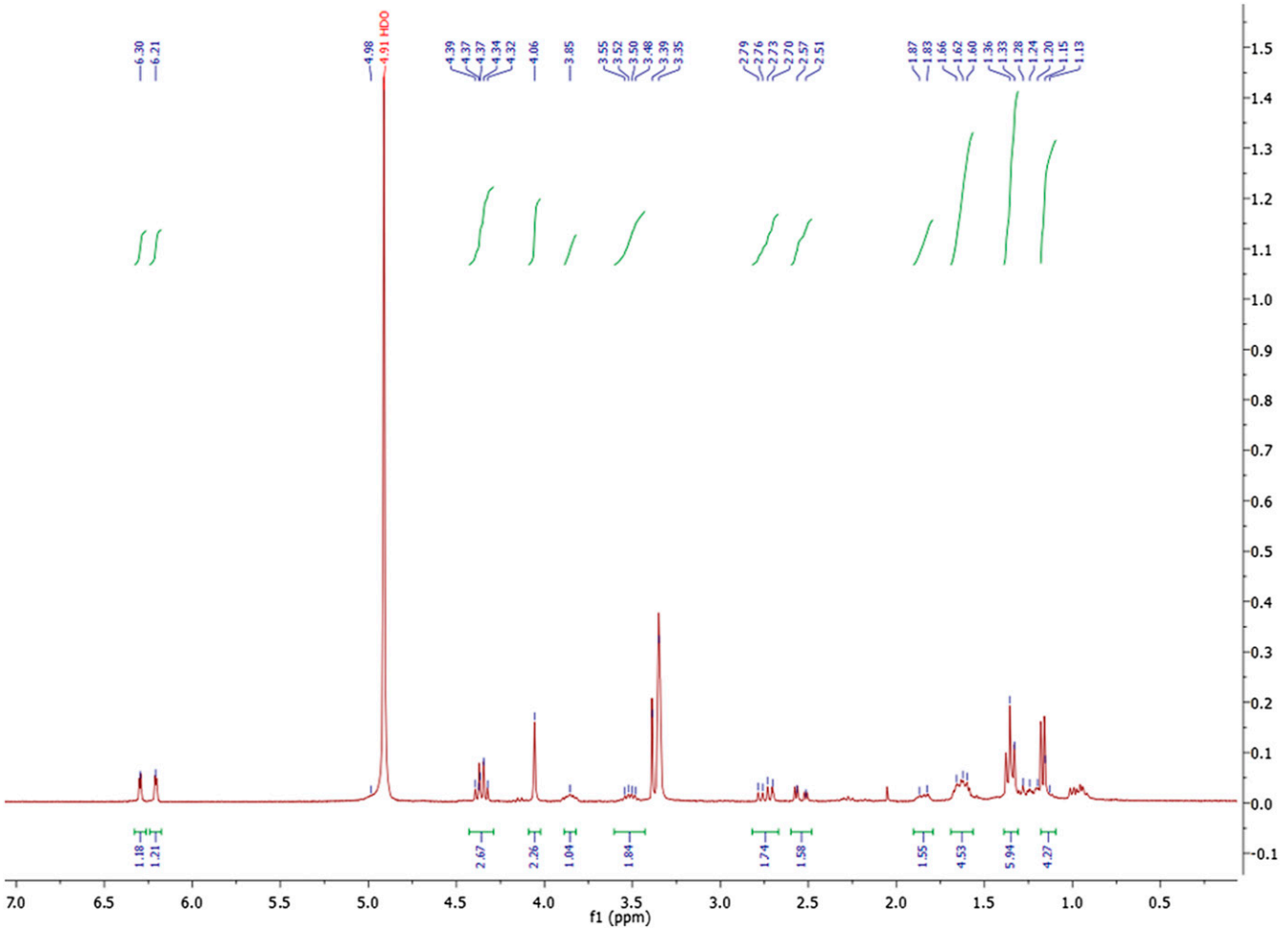

Fig. S7. ^{1}H NMR spectrum of **10**.

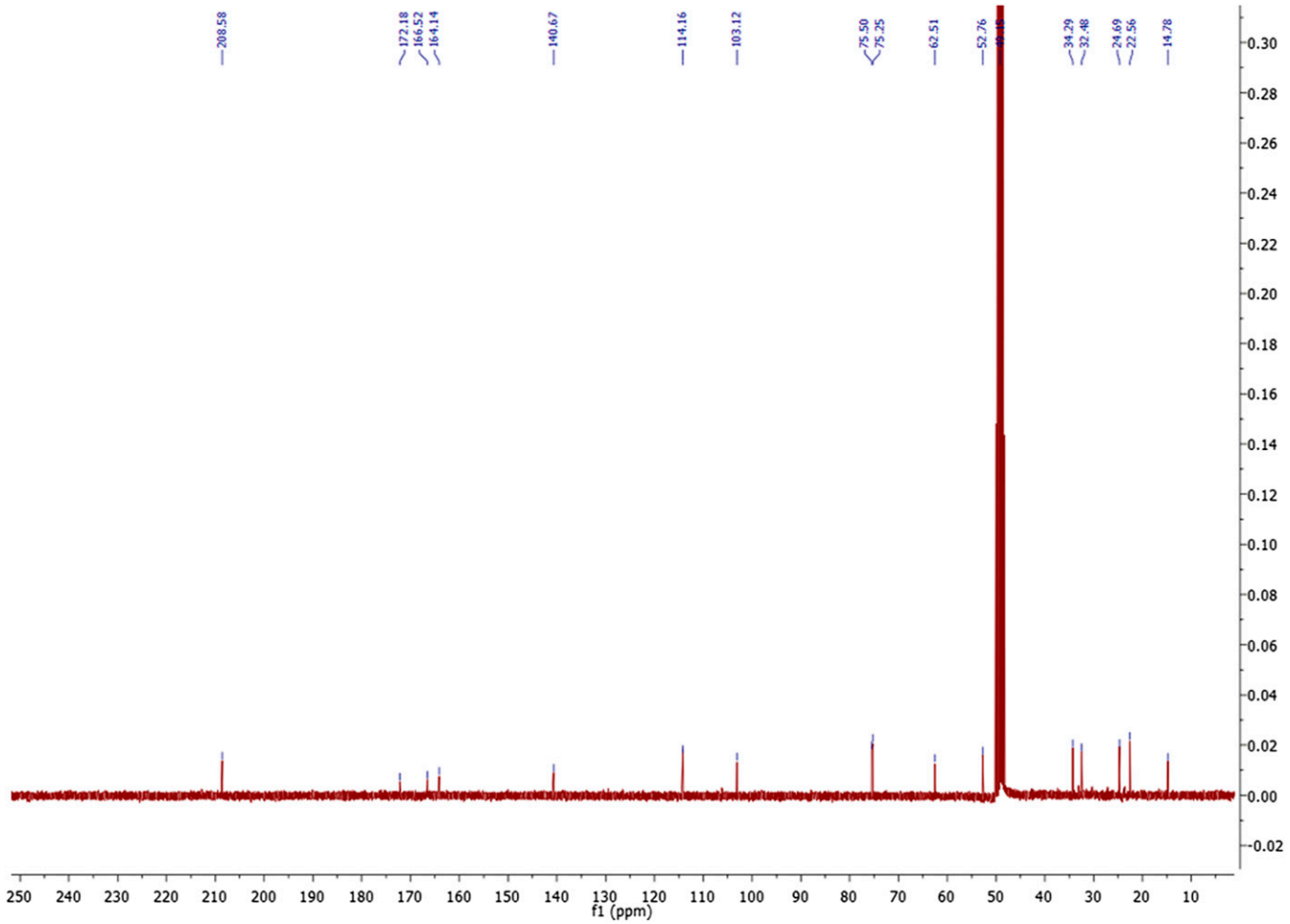

Fig. S8. ^{13}C NMR spectrum of **10**.

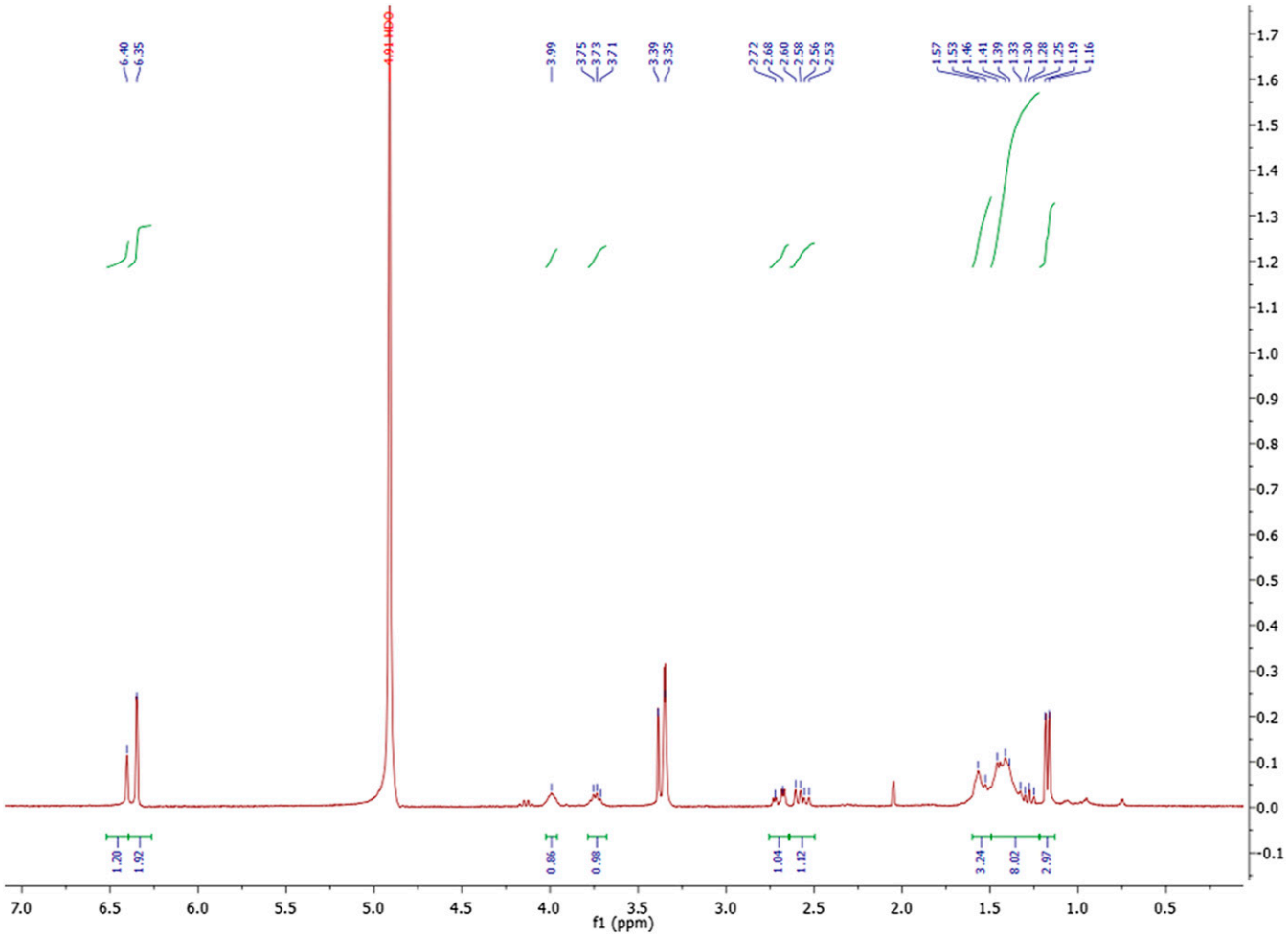

Fig. S9. ^{1}H NMR spectrum of **11**.

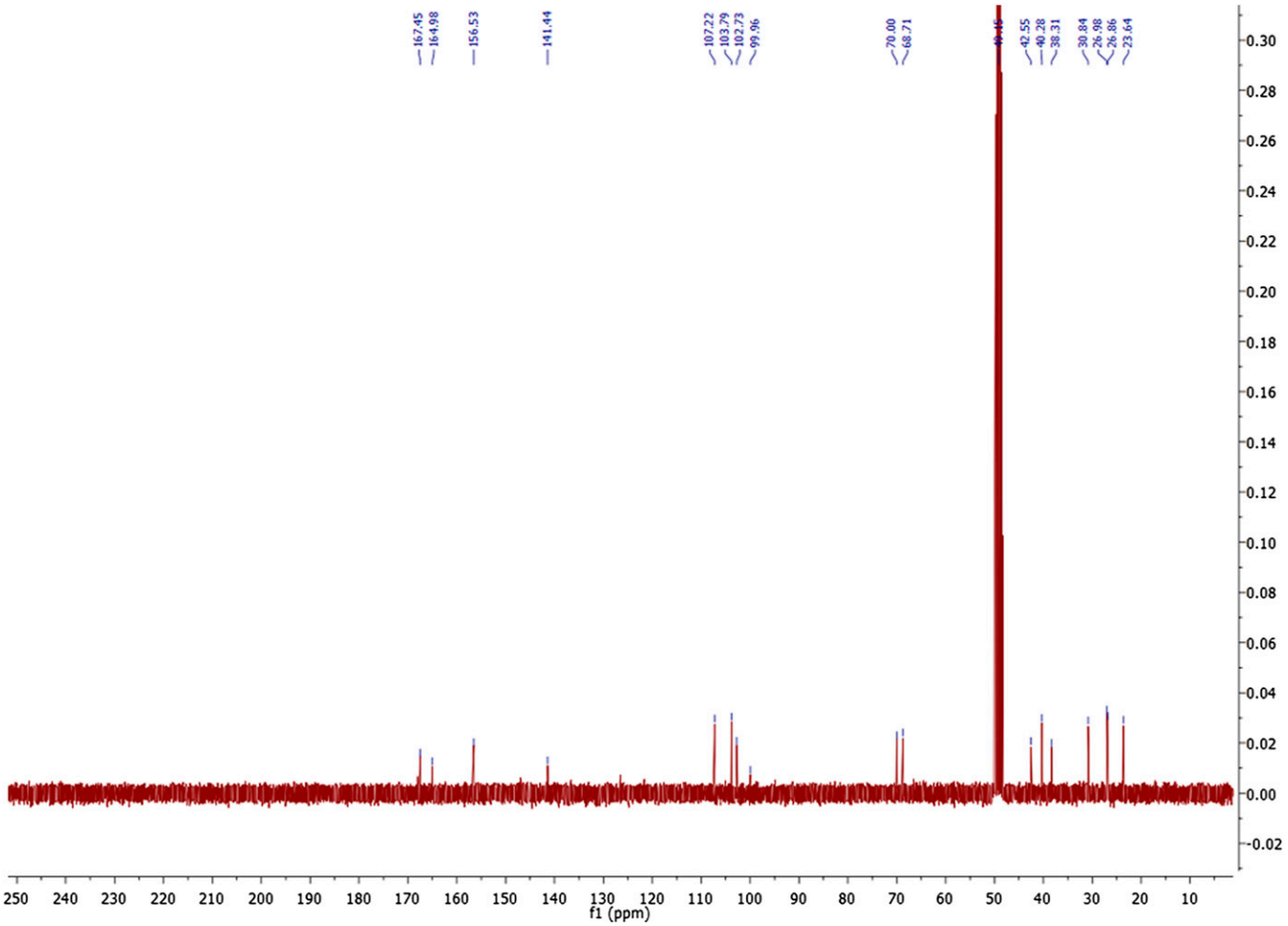

Fig. S10. ^{13}C NMR spectrum of **11**.

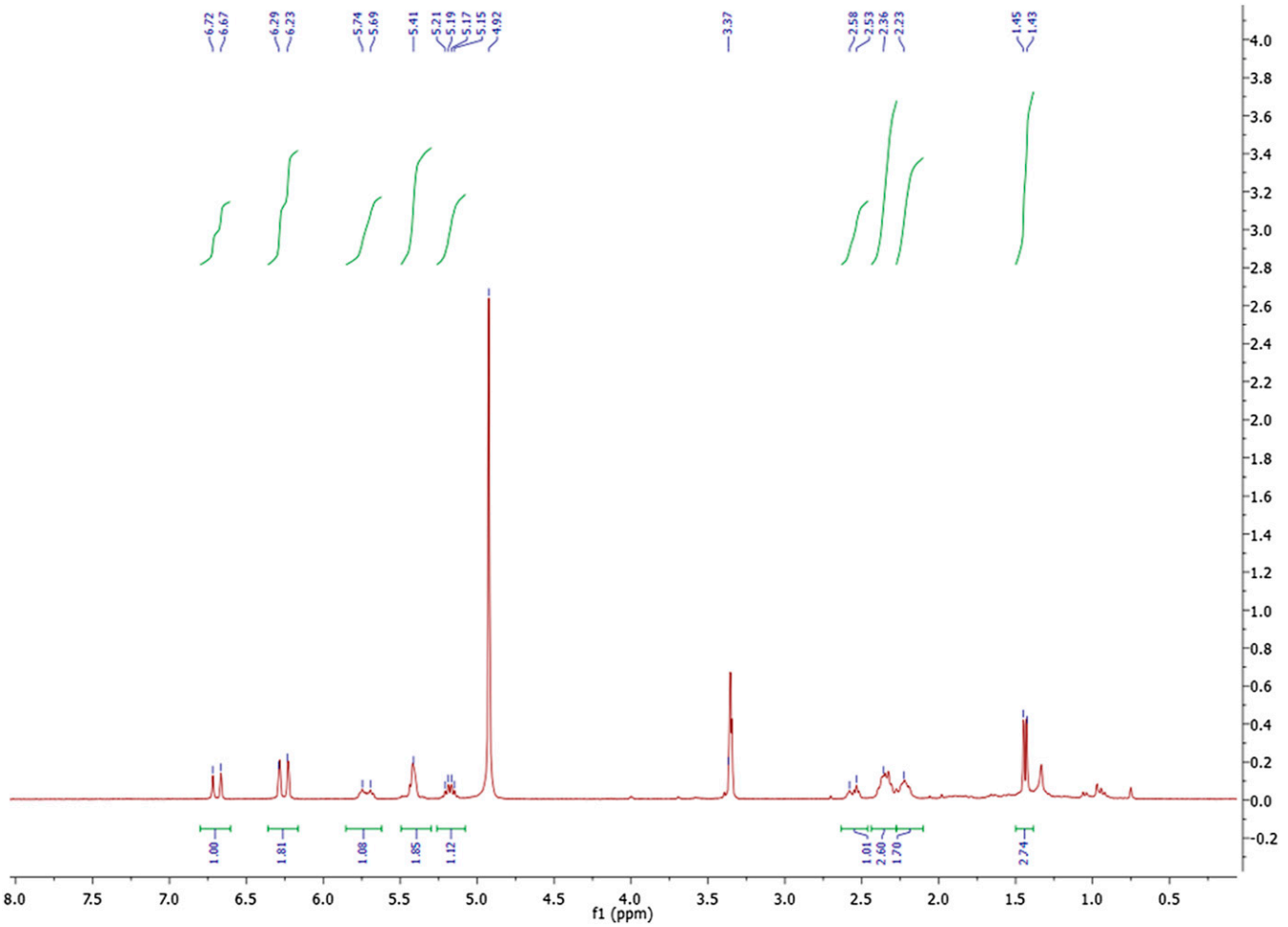

Fig. S11. ^{1}H NMR spectrum of **12**.

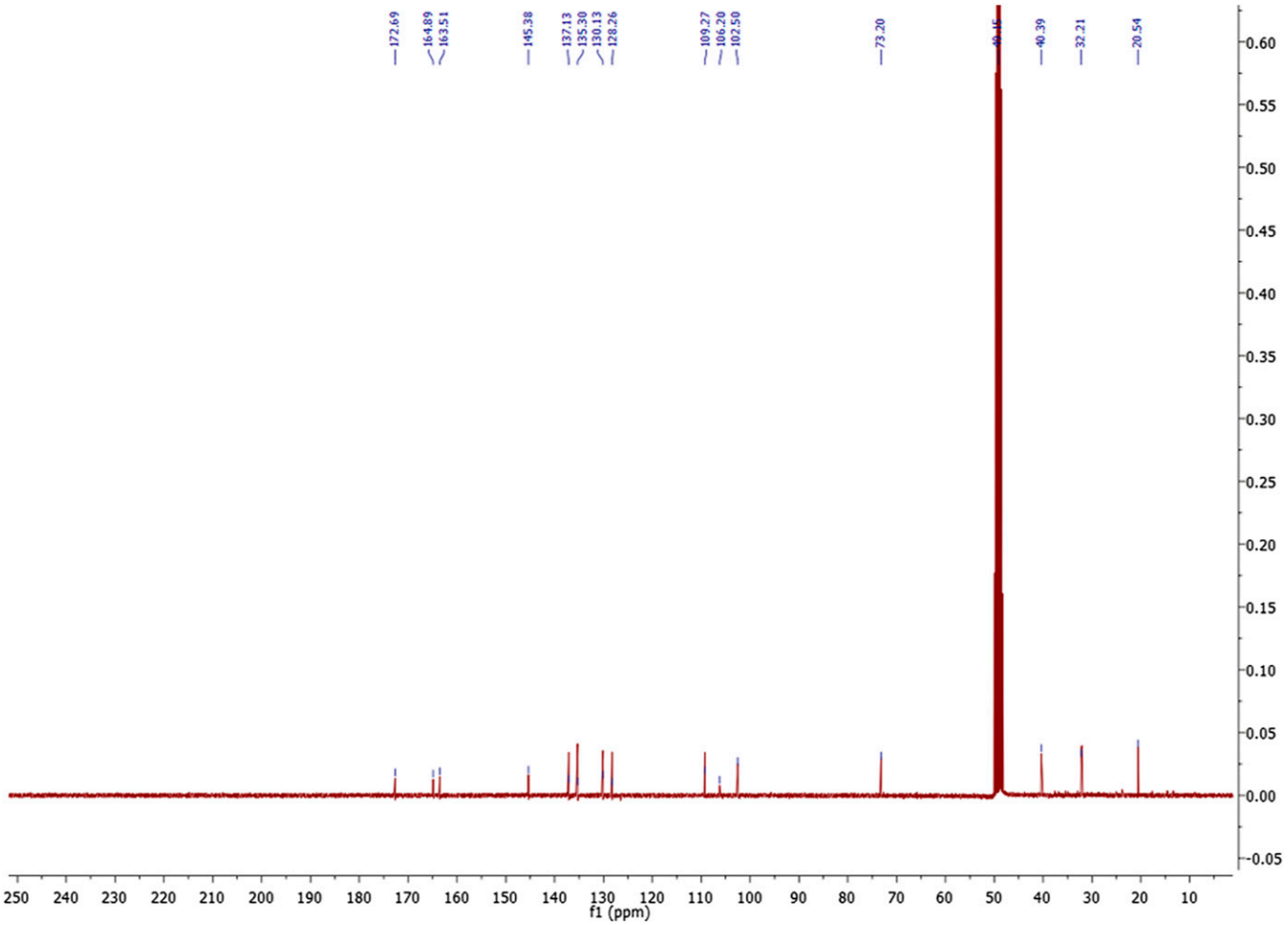

Fig. S12. ^{13}C NMR spectrum of **12**.

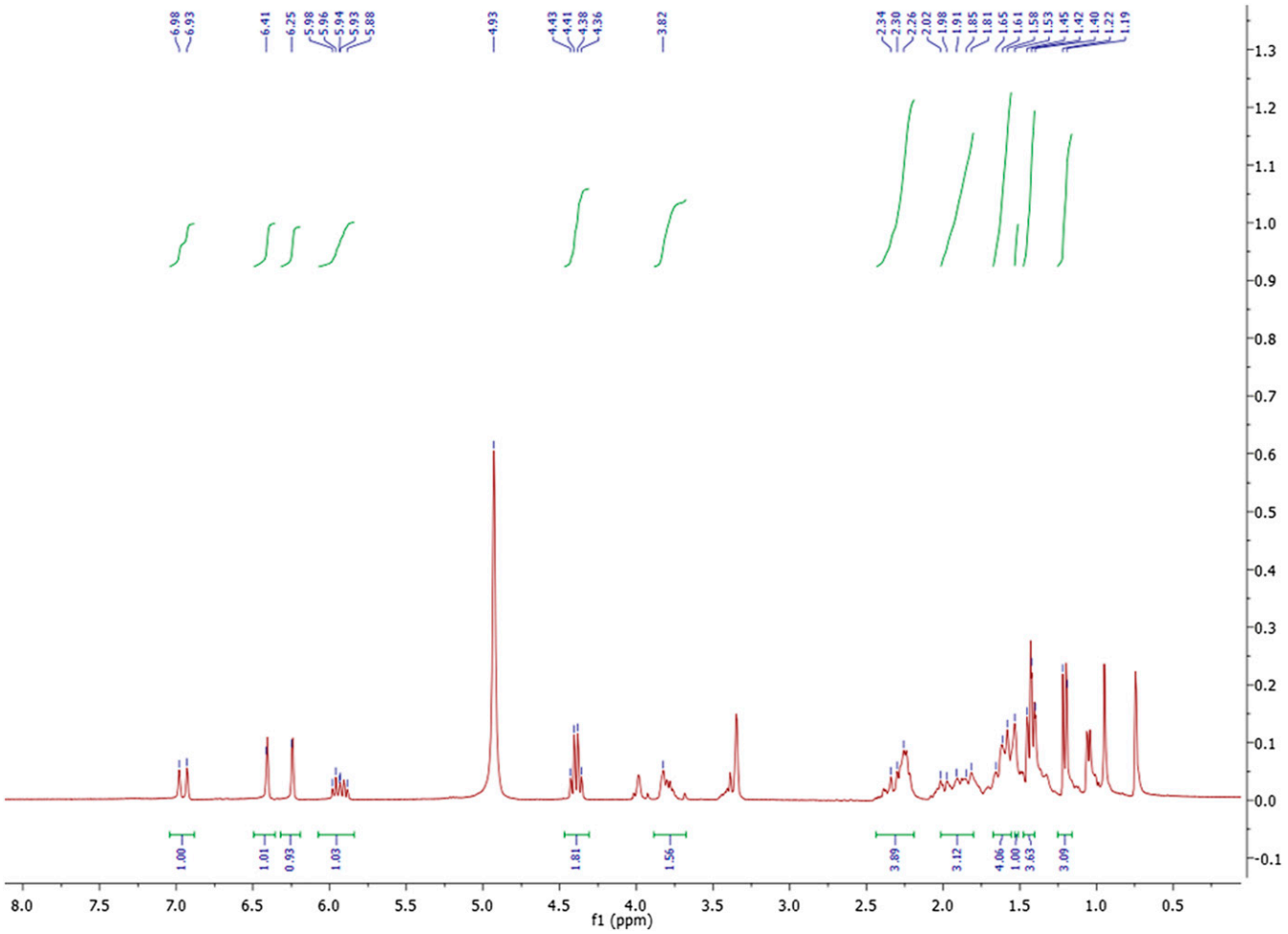

Fig. S13. ^{1}H NMR spectrum of **13**.

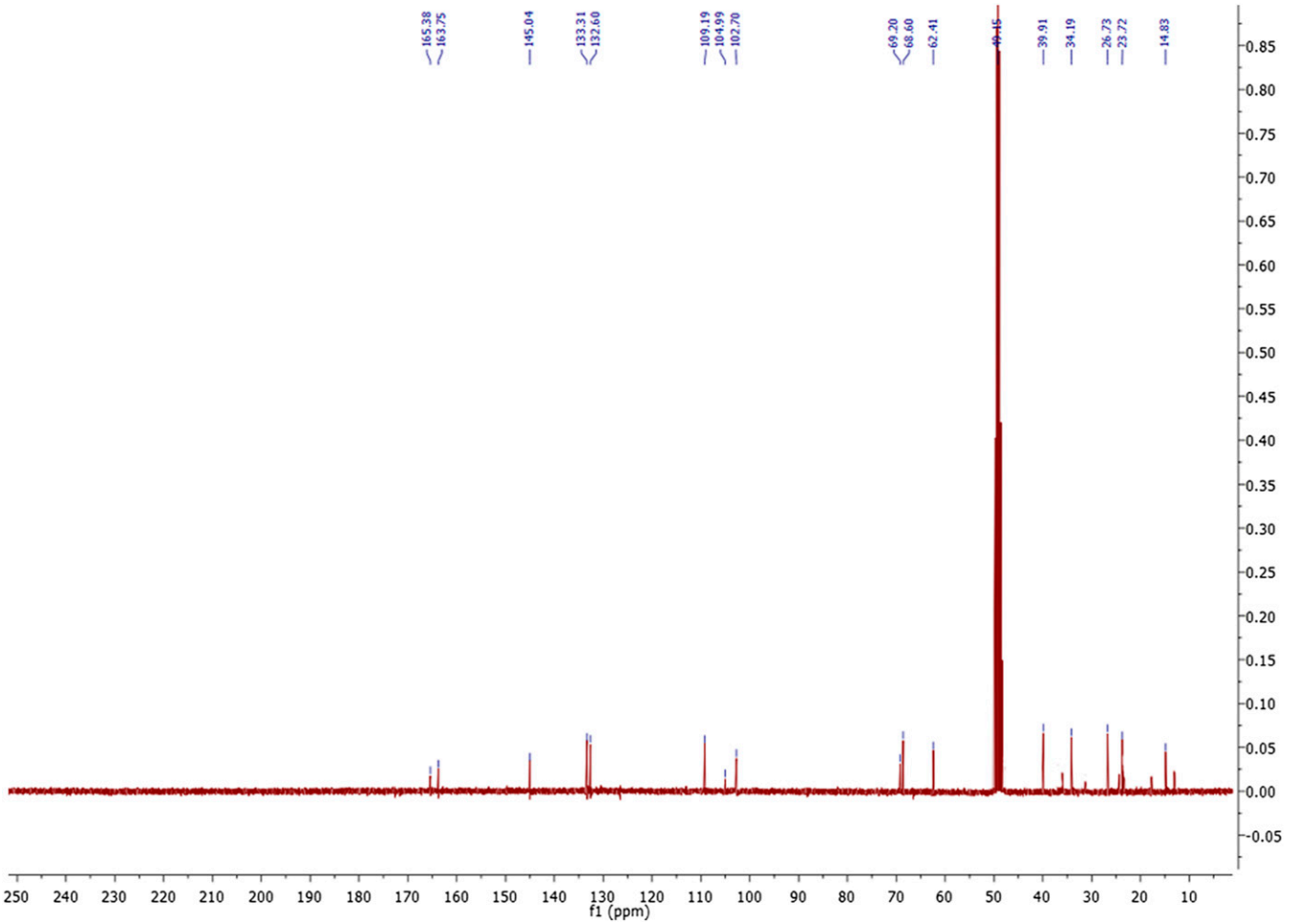

Fig. S14. ^{13}C NMR spectrum of **13**.

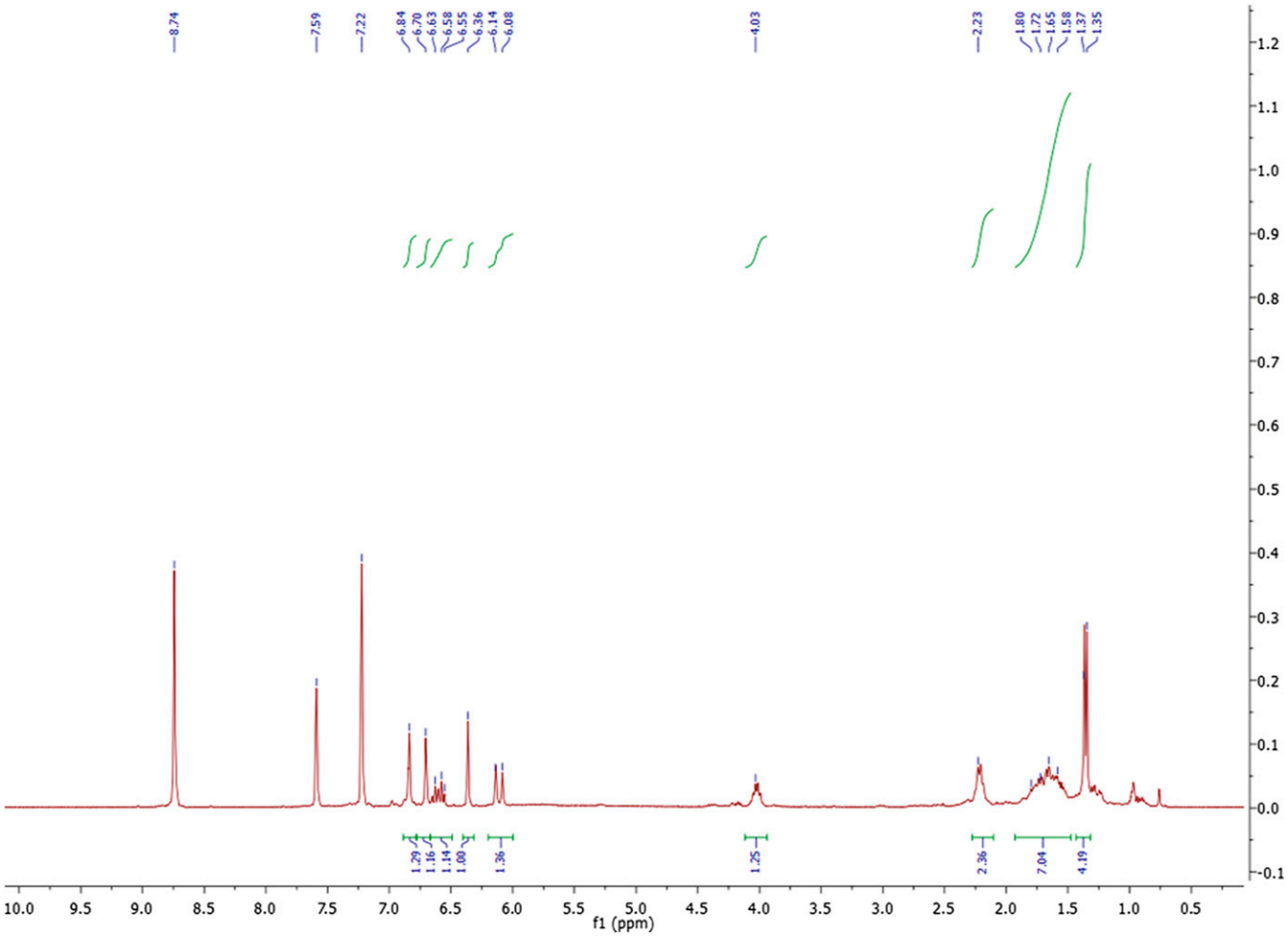

Fig. S15. ^{1}H NMR spectrum of **14**.

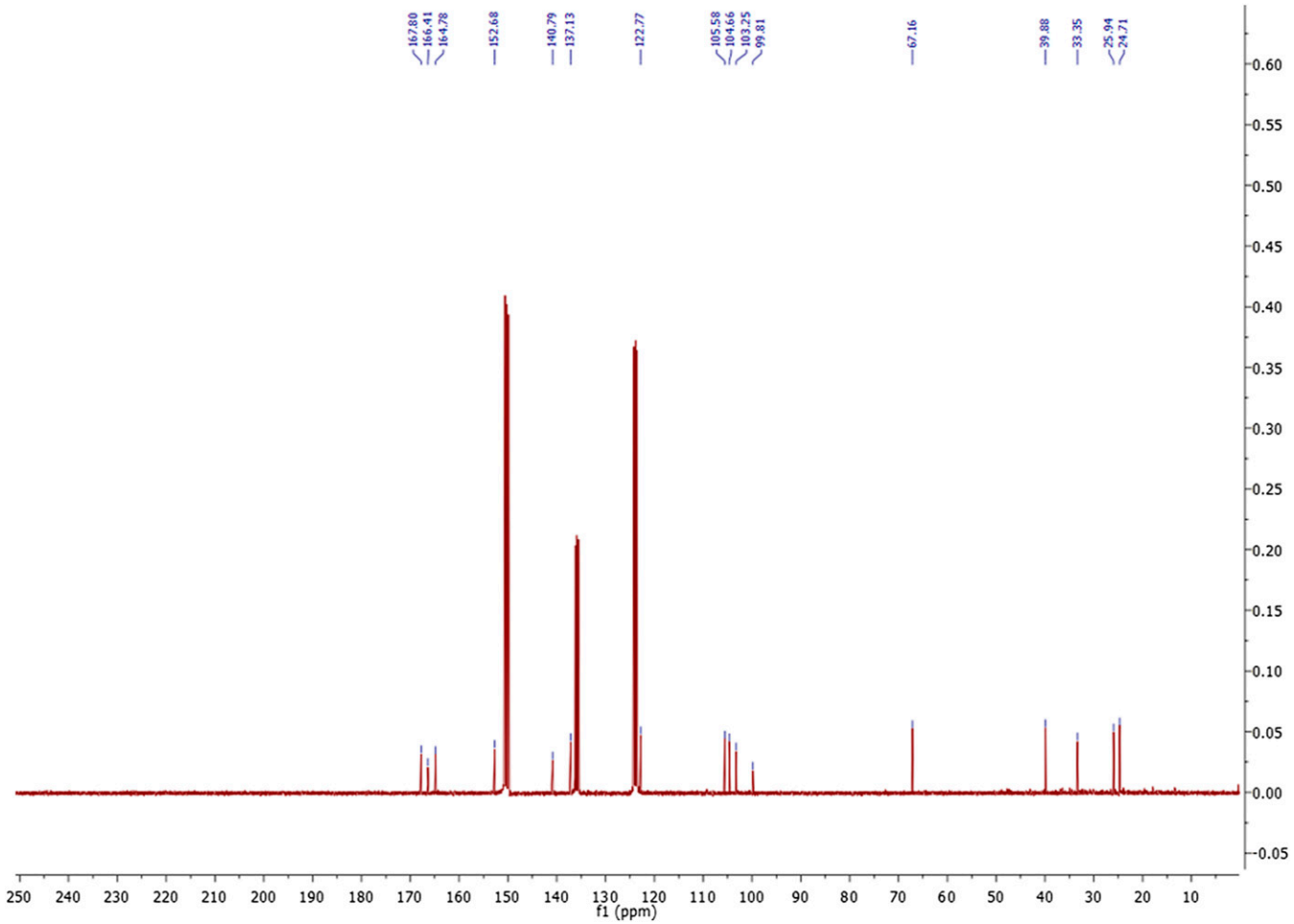

Fig. S16. ^{13}C NMR spectrum of **14**.

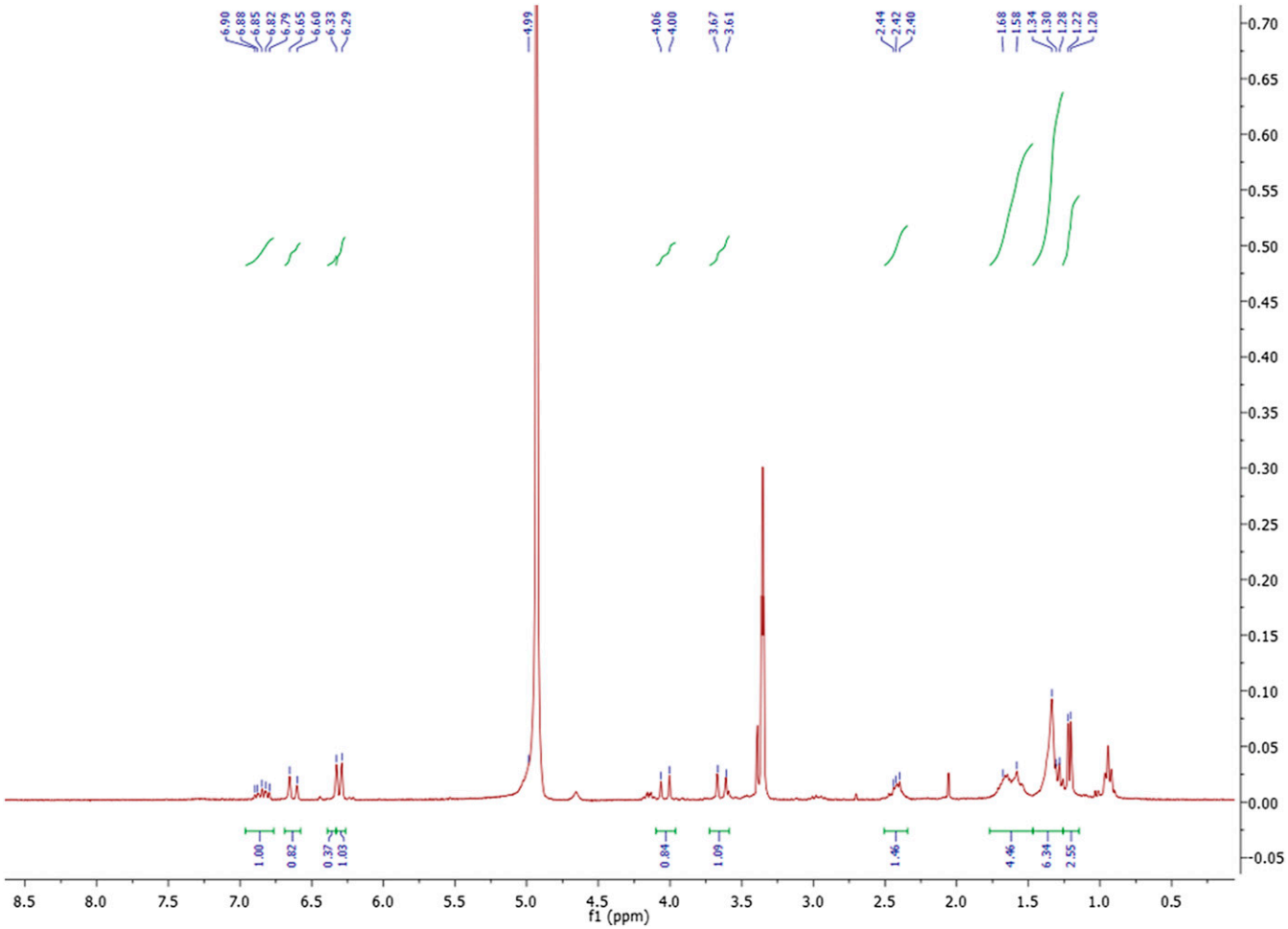

Fig. S17. ^{1}H NMR spectrum of **16**.

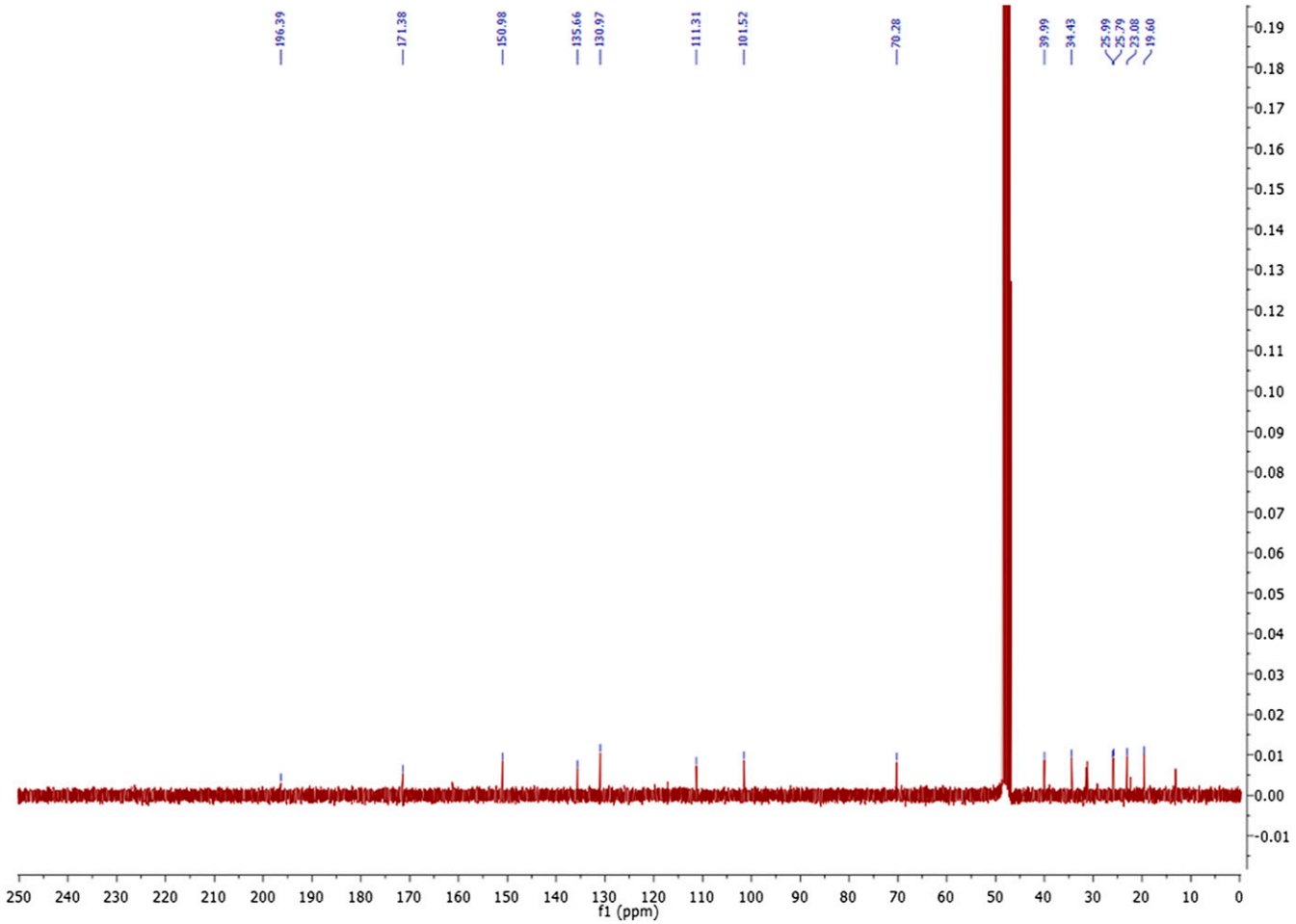

Fig. S18. ^{13}C NMR spectrum of **16**.

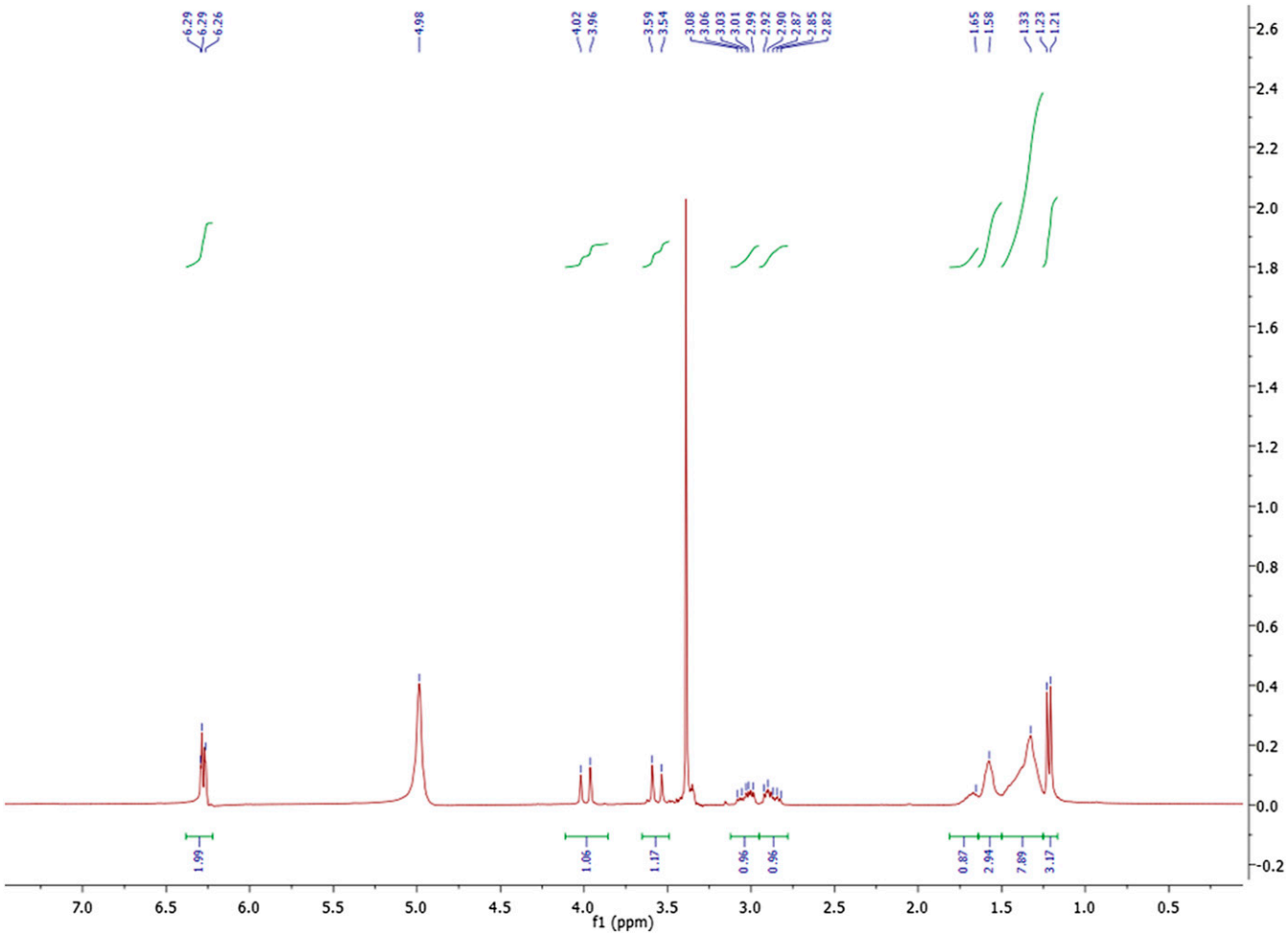

Fig. S19. ^{1}H NMR spectrum of **17**.

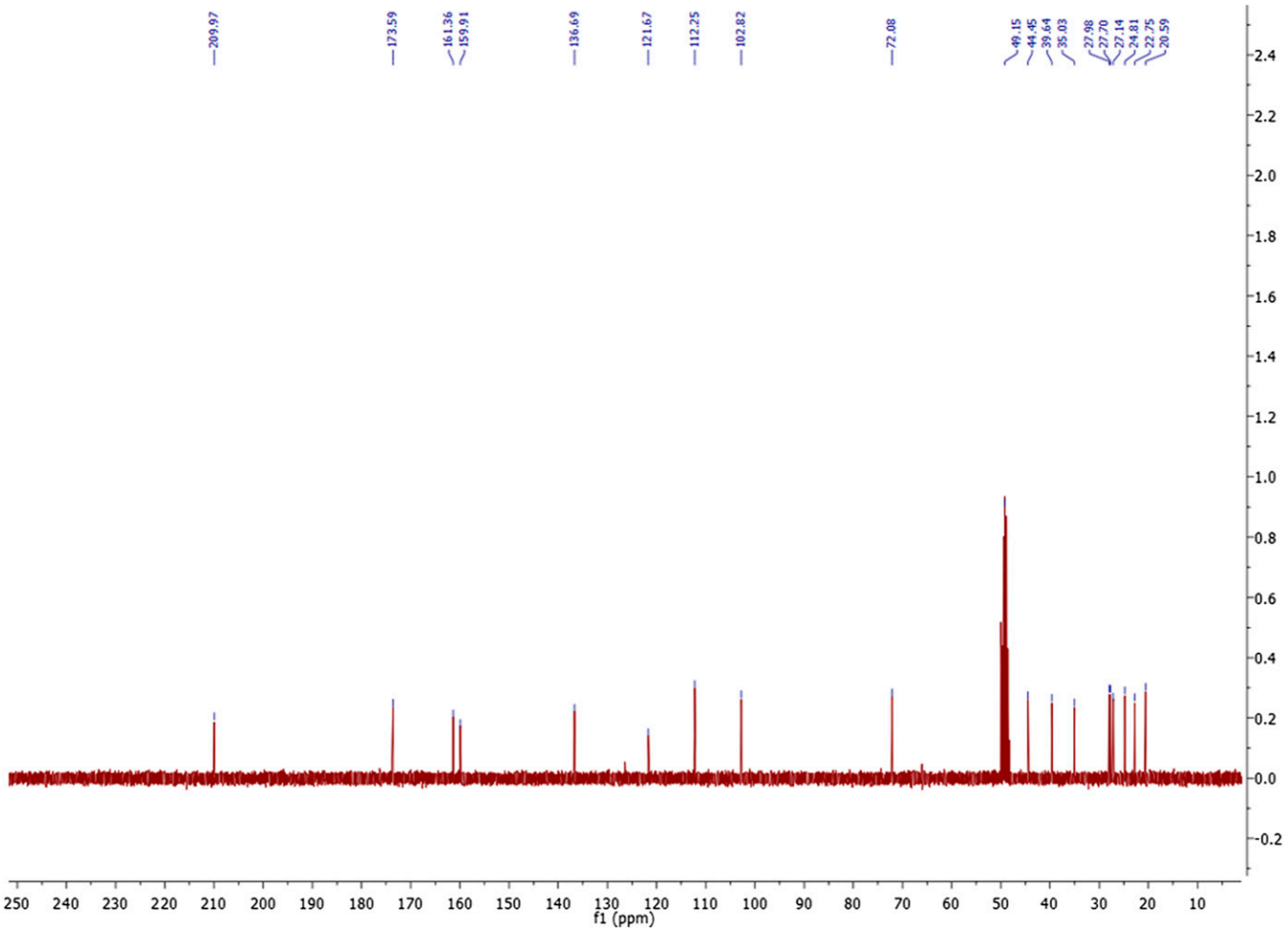

Fig. S20. ^{13}C NMR spectrum of **17**.

Table S1. PCR primers used in this study

Primer name	Sequence
At_SAT_to_Cc_F (NdeI)	5′-CTTCATATGGACTCCAACCGTCCTGC-3′
At_SAT_to_Cc_R	5′-GCGATGATGATGTTGATAC GGTTGGTGGCTTCGCAGTG-3′
Cc_SAT_Dn_F	5′-GTATCAACATCATCATCGCAAAGTGG-3′
Cc_SAT_Dn_R (AgeI)	5′-AGGCGAACCGGTGCGGATG-3′
SAT_Up_F (NdeI)	5′-GGACTACAAAGACGATGACGACAAGCTTC-3′
At_SAT_to_Cc_Up_R	5′-ATGTTGATACCGAGGCCTG CGCAGTGATCCTATCCTGG-3′
At_SAT_to_Cc_Dn_F	5′-CAGGCCTCGGTATCAACATCATCATC-3′
Cc_Dn_R (AgeI)	5′-ATCAACTCTTGGGTACTTGACGCAGTGC-3′
Cc_SAT_to_At_F (NdeI)	5′-GCTTCATATGTCTAGGCTACCACAGAAG-3′
Cc_SAT_to_At_R	5′-ATCCCGTCTCGACTGTCTGGCGAGGCCTGAAGAAGGGAC-3′
At_SAT_Dn_F	5′-CCAGACAGTCGAGACGGGATCGC-3′
At_SAT_Dn_R (Bsu36I)	5′-AGAATTGGCCTTGATAGCCCCGAC-3′
Cc_SAT_Up_R	5′-GAGCTTTGTTTGTTCCAG CGAGGCCTGAAGAAGGGAC-3′
Lass_Dn_F	5′-CTGGAACAAACAAAGCTCCCCGG-3′
Lass_Dn_R (HpaI)	5′-ATGCATGCATTCCCACCCGCTG-3′
At_SAT_Up_R	5′-GAGCTTTGTTTGTTCCAGCGCAGTGATCCTATCCTGGAG-3′
Ress_SAT_Up_R	5′-GAGCTTTGTTTGTTCCAG ATCTGTCTCTGCCTGTGCATG-3′

Table S2. ^{1}H (300 MHz) and ^{13}C (75 MHz) NMR data for 10, 11, and 12 (CD_3OD, δ in ppm, *J* in Hz)

	10		11		12	
No.	δ_C	δ_H	δ_C	δ_H	δ_C	δ_H
1	170.6		166.1		172.7	
2	104.8		98.7		106.2	
3	162.7		163.5		164.9	
4	101.6	6.16 (1H, d, 2.4)	101.2	6.32 (1H, s)	102.5	6.18 (1H, s)
5	164.9		166.0		163.5	
6	112.7	6.25 (1H, d, 2.4)	102.3	6.14 (1H, s)	109.2	6.24 (1H, s)
7	139.2		140.1		145.4	
8	51.2	4.02 (2H, s)	105.7	6.37 (1H, s)	137.1	6.64 (1H, d, 15.6)
9	207.1		155.0		130.1	6.59 (1H, dt, 15.6, 5.8)
10	52.2	2.71 (1H, dd, 16.5, 7.9) 2.50 (1H, dd, 16.5, 4.8)	41.5	2.67 (1H, dd, 14.8, 4.5) 2.54 (1H, dd, 14.8, 8.2)	32.2	2.31 (1H, m) 2.17 (1H, m)
11	73.8	3.80 (1H, m)	68.5	3.96 (1H, m)	32.1	2.31 (1H, m) 2.17 (1H, m)
12	31.0	1.59 (1H, m) 1.20 (1H, m)	37.4	1.54 (2H, m)	135.2	5.40 (1H, m)
13	23.2	1.81 (1H, m) 1.58 (1H, m)	25.3	1.41 (2H, m)	128.2	5.40 (1H, m)
14	32.8	1.56 (1H, m) 1.23 (1H, m)	29.3	1.41 (2H, m)	40.4	2.30 (1H, m) 2.48 (1H, m)
15	74.0	3.47 (1H, m)	25.1	1.41 (2H, m)	73.2	5.13 (1H, m)
16	21.0	1.12 (3H, d, 6.2)	38.7	1.39 (2H, m)	20.5	1.39 (3H, d, 6.3)
17	62.0	4.36 (2H, q, 7.2)	67.2	3.72 (1H, m)		
18	14.3	1.36 (3H, t, 7.2)	22.2	1.14 (3H, d, 6.2)		

Table S3. ^{1}H (300 MHz) and ^{13}C (75 MHz) NMR data for 13, 14, 16, and 17 (13, 16 and 17 in CD_3OD; 14 in pyridine-d_5. δ in ppm, *J* in Hz)

	13		14		16		17	
No.	δ_C	δ_H	δ_C	δ_H	δ_C	δ_H	δ_C	δ_H
1	172.7		166.4		171.4		173.6	
2	104.5		99.8		48.3	3.99 (1H, d, 18.6) 3.60 (1H, d, 18.6)	35.1	3.95 (1H, d, 17.1) 3.52 (1H, d, 17.1)
3	165.4		164.8		135.6		136.7	
4	102.7	6.20 (1H, s)	105.6	6.83 (1H, s)	111.3	6.29 (1H, s)	112.7	6.24 (1H, s)
5	163.8		167.8		162.2		161.3	
6	109.2	6.37 (1H, s)	104.7	6.70 (1H, s)	101.5	6.25 (1H, s)	102.8	6.22 (1H, s)
7	145.0		140.8		162.0		159.8	
8	132.6	6.92 (1H, d, 15.4)	103.2	6.36 (1H, s)	117.5		121.8	
9	133.3	5.88 (1H, dt, 15.4, 6.5)	152.7		196.3		210.0	
10	34.2	2.20 (2H, m)	122.8	6.11 (1H, d, 15.4)	130.9	6.59 (1H, d, 15.1)	44.5	3.00 (1H, ddd, 16.1, 8.3, 4.1) 2.84 (1H, ddd, 16.1, 6.9, 4.1)
11	26.7	1.40 (2H, m)	137.1	6.60 (1H, m)	150.9	6.80 (1H, m)	28.0	1.40 (2H, m)
12	39.9	1.61 (2H, m)	33.3	2.23 (2H, m)	34.4	2.36 (2H, m)	24.8	1.29 (2H, m)
13	69.2	3.77 (1H, m)	25.9	1.77 (1H, m) 1.69 (1H, m)	25.9	1.59 (2H, m)	27.7	1.29 (2H, m)
14	23.7	1.17 (3H, d, 6.2)	39.9	1.67 (1H, m) 1.56 (1H, m)	25.7	1.29 (2H, m)	27.1	1.29 (2H, m)
15	62.4	4.34 (2H, q, 7.2)	67.1	4.02 (1H, m)	19.6	1.29 (2H, m)	22.7	1.36 (2H, m)
16	14.8	1.38 (3H, t, 7.2)	24.7	1.35 (3H, d, 6.0)	39.9	1.67 (1H, m) 1.26 (1H, m)	39.6	1.66 (1H, m) 1.30 (1H, m)
17					70.3	4.99 (1H, m)	72.0	4.95 (1H, m)
18					23.1	1.17 (3H, d, 6.2)	20.6	1.18 (3H, d, 6.2)